Integrative Biology, 2023, **15**, 1–14
https://doi.org/10.1093/intbio/zyad013
Original Article

Human enteroids as a tool to study conventional and ultra-high dose rate radiation

Katarina C. Klett[1], Briana C. Martin-Villa[2], Victoria S. Villarreal[3], Stavros Melemenidis[4], Vignesh Viswanathan[4], Rakesh Manjappa[4], M. Ramish Ashraf[4], Luis Soto[4], Brianna Lau[4], Suparna Dutt[4], Erinn B. Rankin[4,5,6], Billy W. Loo Jr[4,6] and Sarah C. Heilshorn[3,*]

[1]Institute for Stem Cell Biology and Regenerative Medicine, Stanford University School of Medicine, Stanford, CA, USA
[2]Department of Bioengineering, Stanford University, Stanford, CA, USA
[3]Department of Materials Science and Engineering, Stanford University, Stanford, CA, USA
[4]Department of Radiation Oncology, Stanford University School of Medicine, Stanford, CA, USA
[5]Department of Obstetrics and Gynecology, Stanford University School of Medicine, Stanford, CA, USA
[6]Stanford Cancer Institute, Stanford University School of Medicine, Stanford, CA, USA

*Corresponding author. E-mail: heilshorn@stanford.edu

Abstract

Radiation therapy, one of the most effective therapies to treat cancer, is highly toxic to healthy tissue. The delivery of radiation at ultra-high dose rates, FLASH radiation therapy (FLASH), has been shown to maintain therapeutic anti-tumor efficacy while sparing normal tissues compared to conventional dose rate irradiation (CONV). Though promising, these studies have been limited mainly to murine models. Here, we leveraged enteroids, three-dimensional cell clusters that mimic the intestine, to study human-specific tissue response to radiation. We observed enteroids have a greater colony growth potential following FLASH compared with CONV. In addition, the enteroids that reformed following FLASH more frequently exhibited proper intestinal polarity. While we did not observe differences in enteroid damage across groups, we did see distinct transcriptomic changes. Specifically, the FLASH enteroids upregulated the expression of genes associated with the *WNT*-family, cell-cell adhesion, and hypoxia response. These studies validate human enteroids as a model to investigate FLASH and provide further evidence supporting clinical study of this therapy.

Insight Box
Promising work has been done to demonstrate the potential of ultra-high dose rate radiation (FLASH) to ablate cancerous tissue, while preserving healthy tissue. While encouraging, these findings have been primarily observed using pre-clinical murine and traditional two-dimensional cell culture. This study validates the use of human enteroids as a tool to investigate human-specific tissue response to FLASH. Specifically, the work described demonstrates the ability of enteroids to recapitulate previous *in vivo* findings, while also providing a lens through which to probe cellular and molecular-level responses to FLASH. The human enteroids described herein offer a powerful model that can be used to probe the underlying mechanisms of FLASH in future studies.

Keywords: organoids; radiation; intestinal repair; FLASH radiation

INTRODUCTION

Radiation therapy is one of the most effective therapeutic modalities against cancer and is required by more than 60% of all patients with cancer during the course of their treatment [1]. Unfortunately, radiation therapy is highly toxic to normal, healthy tissue and is known to have many negative side effects ranging from fatigue and hair loss to heart complications, lung damage, and enteritis depending on the treated body site [2–7]. Radiation is especially toxic to intestinal tissue, which is prone to damage due to its constant renewal and location adjacent to areas that often require radiation, like the pelvis and abdomen [8–10]. Thus, the dose—and efficacy—of radiation therapy is limited by the maximum amount of damage that the surrounding healthy tissue can tolerate [11]. Recently, several new techniques have been developed to ensure delivery of as high a radiation dose as possible to the tumor site while causing as little damage as possible to the surrounding healthy tissue [12–19].

One promising radiation modality under development, termed FLASH radiation therapy (FLASH), is defined as the delivery of ultra-high dose rates of radiation (e.g. > 40 Gy/s) compared to conventional dose rate radiation therapy (CONV, typically ~0.1 Gy/s). This allows delivery of equivalent radiation doses over a shorter period of time, often in the millisecond range. In preclinical studies, FLASH achieves tumor eradication with fewer side effects [20]. In the intestines specifically, abdominal FLASH irradiation of mice preserved the number of regenerating intestinal crypts compared to CONV, while maintaining efficacy against tumors

Received: July 16, 2023. **Revised:** September 22, 2023. **Accepted:** September 26, 2023

[21–25]. Additionally, the FLASH-irradiated mice were able to produce stool at rates more similar to non-irradiated mice, an indication of intestinal health. Healthy intestinal tissue structure was better maintained following FLASH compared CONV [21–27], and animals were able to regain weight more quickly. This phenomenon of fewer side effects following FLASH has been termed the "FLASH-effect" [20]. If proven to be both safe and effective in clinical trials, FLASH could overcome the limitations of CONV, significantly improving both the life expectancy and quality of life of patients with cancer worldwide.

To date, two clinical reports describe successful use of FLASH to treat patients with T-cell lymphoma or bone metastasis with minimal toxicity [28, 29]. While these studies suggest that FLASH is technically feasible to deliver in selected clinical settings, additional preclinical and clinical investigations are needed to fully understand the efficacy and safety of FLASH and the potential underlying mechanisms responsible for the FLASH-effect.

Although pre-clinical animal studies are necessary to study FLASH, animals have clear anatomical, cellular, and molecular differences from humans [30–33]. In the intestines specifically, there are known distinctions between the clonal dynamics of the crypt [34] and potential differences in repair mechanisms [35] between mice and humans. In addition, there is an increasing public and governmental push to reduce scientific reliance on animal research. This movement is evidenced by the United States Food and Drug Administration's recent recommendation to phase out animal testing and increase use of human tissue models [36]. In response, the biomedical community has turned to advanced three-dimensional cultures as human-mimetic *in vitro* alternatives that can be easily manipulated for hypothesis-driven analyses and can be expanded for high-throughput assays [37, 38].

In this study, we validated the use of murine and human intestinal enteroid cultures as a tool to study the effects of FLASH and CONV on healthy tissue. Enteroids are three-dimensional clusters of cells that mimic the epithelium of native small intestinal tissue. Specifically, enteroids contain multiple intestinal cell types including intestinal stem and progenitor cells. These multicellular cultures self-organize into spherical, hollow structures that spontaneously polarize to have an internal lumen, similar to the gut tube. Because enteroids can be isolated from primary human tissue, they provide a powerful lens to study how FLASH impacts human tissue specifically. When kept in a more immature state, these enteroids are highly proliferative and can be used in colony formation assays to quantify their regenerative repair potential.

Ionizing radiation is known to be especially damaging to proliferating cells, as those cells often have greater levels of exposed DNA and are unable to respond as quickly to repair damage [39]. This often leads to cell death, as a means of preventing damaged DNA from being passed onto progeny. This damage is a result of highly reactive free radical formation, including reactive oxygen species (ROS), that damage DNA, lipids, carbohydrates, and proteins [40, 41]. Currently, many hypotheses have been proposed to explain potential mechanisms that might mediate the FLASH-effect, a number of which can be readily tested in this *in vitro* model. These theories include 1) a decrease in oxidative damage in healthy cells [42, 43], 2) preservation of the stem cell niche [44, 45], and 3) the induction of radio-protective tissue hypoxia [46–50]. In our human enteroid model, we observed cellular and molecular evidence for several of these potential mechanisms, suggesting that multiple pathways may contribute to the FLASH-effect seen in animal models.

RESULTS

FLASH-irradiated enteroids exhibit greater colony growth potential than CONV-irradiated enteroids

All irradiations were performed on a clinical linear accelerator (LINAC) that was configured to produce a 16 MeV electron beam capable of delivering uniform doses across a well-plate (Fig. 1A, Fig. S1, Table S1). Delivered radiation doses were measured *via* radiochromic film during each radiation. These measurements confirmed that the machine was capable of achieving accurate doses of radiation using both CONV and FLASH protocols (Fig. 1B). All FLASH radiations were performed at dose rates above 100 Gy/s, whereas CONV radiations were below 0.2 Gy/s (Fig. 1C, Table S2). Although dose rates were substantially different between CONV and FLASH, the same total dose was maintained across samples, allowing us to compare tissue responses between the two radiation protocols.

Intestinal enteroids were isolated from either healthy primary murine or healthy patient intestinal duodenum, the most radiosensitive portion of the intestines [51]. After encapsulation of single cells within a three-dimensional basal lamina matrix, the cultures form enteroids over 2–6 days, which we define as multicellular spheres with an internal, polarized lumen. Polarization is confirmed by the appearance of apical zonal occludens (ZO-1) along with ß-catenin staining at cell-cell junctions and the basal surface (Fig. 1D, [52]). At this stage, the enteroids are highly proliferative, as evidenced by expression of the marker Ki67, and express the intestinal progenitor marker, SOX9 (Fig. 1D, Fig. S2, [53, 54]). These intestinal progenitor cells, which are localized to the crypt of the native intestines, are known to be highly sensitive to radiation. As further evidence of their progenitor-like phenotype, we exposed the immature enteroids to differentiation medium and confirmed that the cells could differentiate into more mature epithelial cell types including Paneth cells, enterocytes, and enteroendocrine cells (Fig. S3). We also performed a hypoxia probe assay to measure transient levels of hypoxia in the unirradiated enteroid cultures over time and observed hypoxia levels (~20–30%) were maintained from early enteroid formation (Day 3) to the time of enteroid irradiation (Day 6) (Fig. S4).

To first determine whether our *in vitro* system could recapitulate the FLASH-effect demonstrated previously in preclinical mouse studies, we irradiated murine enteroids with doses spanning 3–8 Gy and subsequently performed a colony formation assay (Fig. S5). This dose range has been previously validated for the irradiation of enteroids [55, 56]. At these low radiation doses, typically changes in organoid viability are not observed [55, 57–59]. Consistent with this, we observed no statistically significant differences in cell viability between unirradiated controls, CONV, and FLASH (Fig. S6). This allowed us to retain a high number of cells post-treatment for downstream analysis of possible differential effects between CONV and FLASH on cell phenotype. For the colony formation assay, irradiated enteroids were dissociated into single cells, which were re-encapsulated and observed by light microscopy over 6 days to observe potential regeneration of enteroids (Fig. 2A). Cells that were FLASH-irradiated maintained the ability to reform enteroids of similar cross-sectional area to the no-radiation control (Fig. 2B–D). The CONV-irradiated cells, however, reformed enteroids that had significantly smaller cross-sectional areas than the no radiation control. We also observed that the CONV-irradiated enteroids did not maintain the symmetric morphology typical of early-stage murine enteroids [60], while

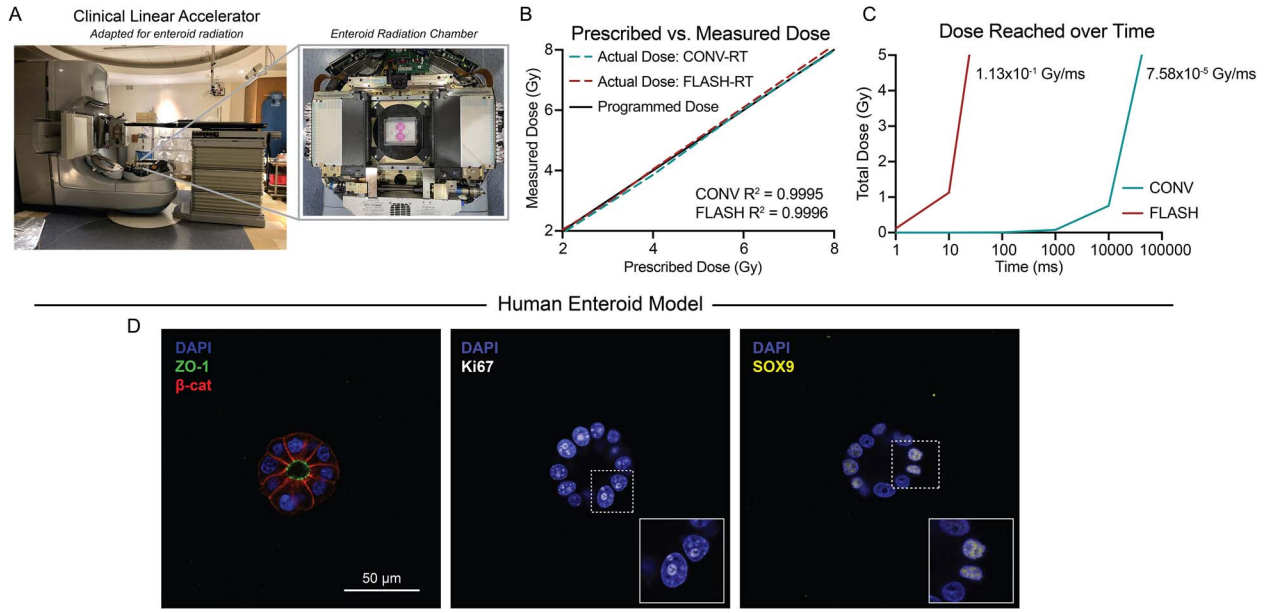

Figure 1. Overview of experimental methodology for linear accelerator (LINAC) radiation of early-stage enteroids. (A) Clinical LINAC adapted for *in vitro* radiation. (B) Accuracy of total dose delivered to enteroid cultures. (C) Time to reach a total 5 Gy dose using either FLASH or CONV. (D) Intestinal crypt-like expression of polarity markers (ZO-1 and ß-catenin), proliferation marker (Ki67), and stemness marker (SOX9). Dashed-lines indicate areas of enlargement. Crypt-like enteroids were irradiated on a LINAC configured for *in vitro* radiation.

spherical morphology was conserved in the reformed FLASH-irradiated enteroids (Fig. 2E).

Driven by these observations of the irradiated murine enteroids, we next investigated whether human enteroids might also exhibit distinct differences following CONV and FLASH in the colony formation assay (Fig. S7). Consistent with other reports, the human enteroid growth rate was slightly slower than that observed for the murine enteroids [61–63]. Similar to the murine colony formation assay, we observed that the FLASH-irradiated human cells were capable of reforming enteroids at similar cross-sectional areas to those formed in the no-radiation control (Fig. 2F–H). The CONV-irradiated cells had significantly smaller cross-sectional areas than both the FLASH and no-radiation culture. Interestingly, we also observed that the human CONV enteroids had significantly fewer ZO1-positive lumens than both the FLASH and no-radiation enteroids, a hallmark of proper enteroid polarization (Fig. 2I).

Damage and repair response of human enteroids to CONV and FLASH

Radiation is known to induce DNA damage and the generation of reactive oxygen species (ROS) [40]. To examine DNA damage and subsequent repair following CONV and FLASH, we irradiated and stained human enteroids for the marker phosphorylated H2A histone family member X (γH2AX), a protein that is recruited to the site of DNA double-strand breaks to initiate repair (Fig. 3A, [64]). Interestingly, we observed that the area of γH2AX foci was not significantly different between the CONV- and FLASH-irradiated enteroids (Fig. 3B and C). Both the CONV- and FLASH-irradiated enteroids had significantly higher localization of γH2AX than the no-radiation control.

We also explored the generation of reactive oxygen species (ROS) following human enteroid radiation. Recognizing that ROS is a core contributor to downstream lipid peroxidation [41], we stained for and quantified levels of lipid peroxidation in the enteroids following radiation. Specifically, we used a commercially available lipid peroxidation kit that involves the addition of linoleic acid (LAA) to the enteroids prior to radiation and quantifies the oxidation of LAA to form a reactive aldehyde upon lipid peroxidation using fluorescently-labeled azide click chemistry. We saw statistically similar levels of lipid peroxidation in the CONV- and FLASH-irradiated enteroids (Fig. 3D and E). Both the CONV- and FLASH-irradiated enteroids had significantly higher levels of lipid peroxidation than the no radiation control, while the positive control of hydrogen peroxide-treated enteroids confirmed validity of the assay.

FLASH-irradiated enteroids are more similar transcriptionally to unirradiated enteroids than CONV-irradiated enteroids

We next compared the transcriptional-level differences between the CONV- and FLASH-irradiated enteroids. Human enteroids were irradiated and then extracted as whole enteroids 1 h later or after a further 96 h of culture for sequencing (Fig. 4A). These timepoints were selected to capture the acute damage and subsequent proliferative phases of intestinal repair following radiation, as previously defined *in vivo* [65].

A principal component analysis (PCA) of our data resulted in two distinct clusters: one cluster of enteroids at 1 h and one at 96 h. Within these two clusters, we observed the FLASH-irradiated enteroids cluster more closely to the no-radiation control than the CONV-irradiated enteroids at both 1 h and 96 h (Fig. 4B, Fig. S8). This is an indication that the expression of the FLASH-irradiated enteroids was more similar to the no-radiation group than the CONV-irradiated enteroids. Next, we leveraged volcano plots to look more closely at gene expression differences between the FLASH- and CONV-irradiated groups specifically (Fig. 4C and D). We observed over 180 and 1100 genes were significantly differentially expressed between these two groups at 1 h and 96 h, respectively ($P < 0.05$, fold change ≥ 1.5).

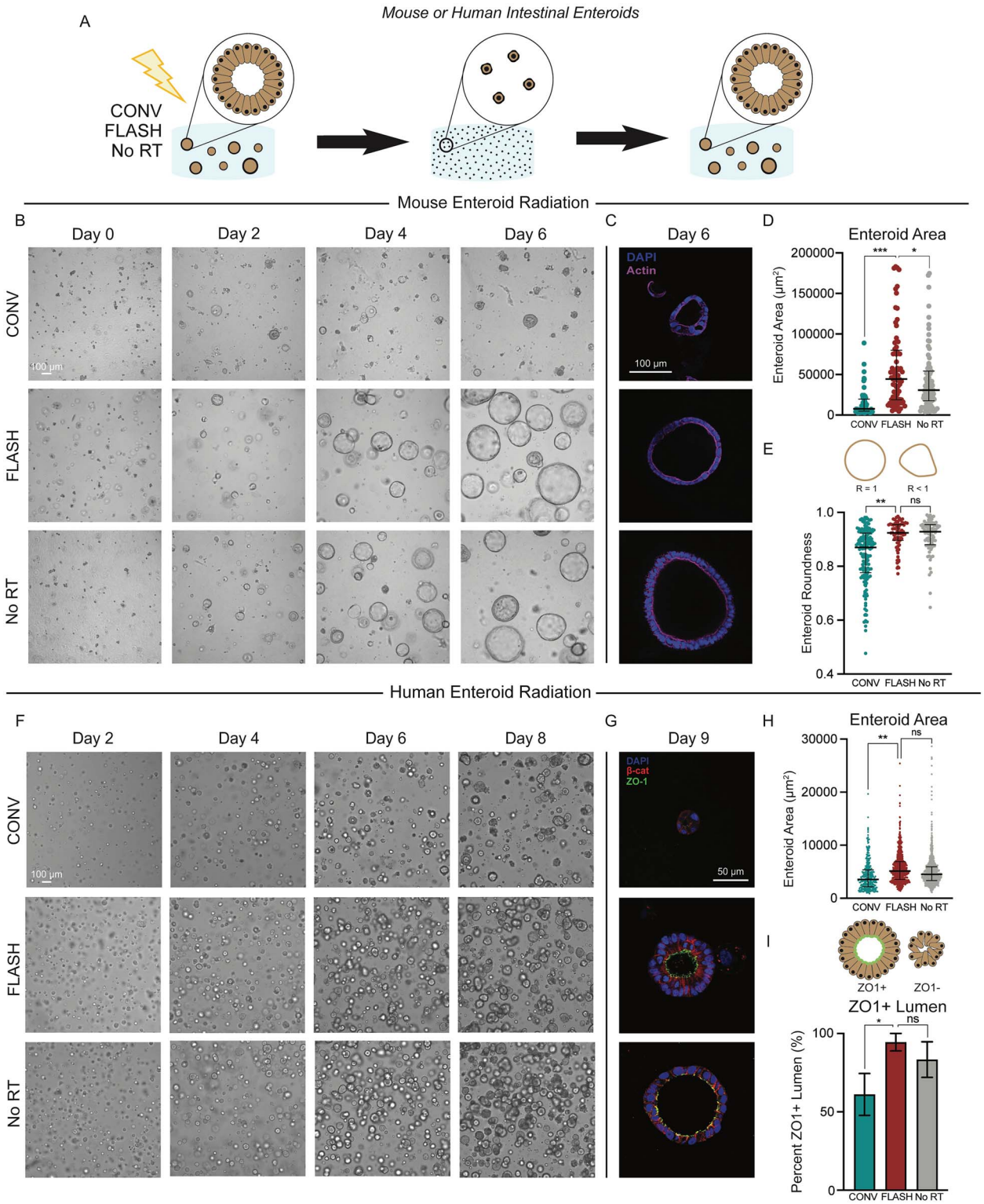

Figure 2. Colony formation assay post-irradiation of murine and human enteroids. (A) Schematic of the enteroid colony formation assay, where enteroids were irradiated, dissociated into single cells, and reseeded within a three-dimensional matrix to assess repair potential. (B) Brightfield images of murine enteroids over time following radiation at 3 Gy. (C) Immunocytochemistry of murine enteroids on day 6, stained for actin to highlight the expected lumen formation. (D) Murine enteroid cross-sectional area 6 days following radiation, where each point is a single enteroid. (E) Quantification of enteroid roundness on day 6, where R = 1 represents a perfect circle, and R < 1 is less symmetric, where each point is a single enteroid. (F) Brightfield images of human enteroids irradiated at 5 Gy over time. (G) Immunocytochemistry of day 9 human enteroids, stained for the markers ZO-1 and ß-catenin. (H) Cross-sectional area of irradiated human enteroids 8 days after radiation, where each point is a single enteroid. (I) Quantification of the presence of ZO-1-positive lumens in human enteroids following radiation. Median with interquartile range, n = 3 independent gel replicates, with n ≥ 19 enteroids per replicate for panels D, E, and n ≥ 95 for panel H. Mean with standard error of the mean, N = 6 independent gel replicates, with n ≥ 3 enteroids per replicate for panel 2I. Two-tailed, unpaired t-tests were performed for statistical analysis, *** = $P < 0.001$, ** = $P < 0.01$, * = $P < 0.05$, ns = not significant. FLASH-irradiated enteroids displayed greater growth potential than CONV and were more likely to reform enteroids with expected structure.

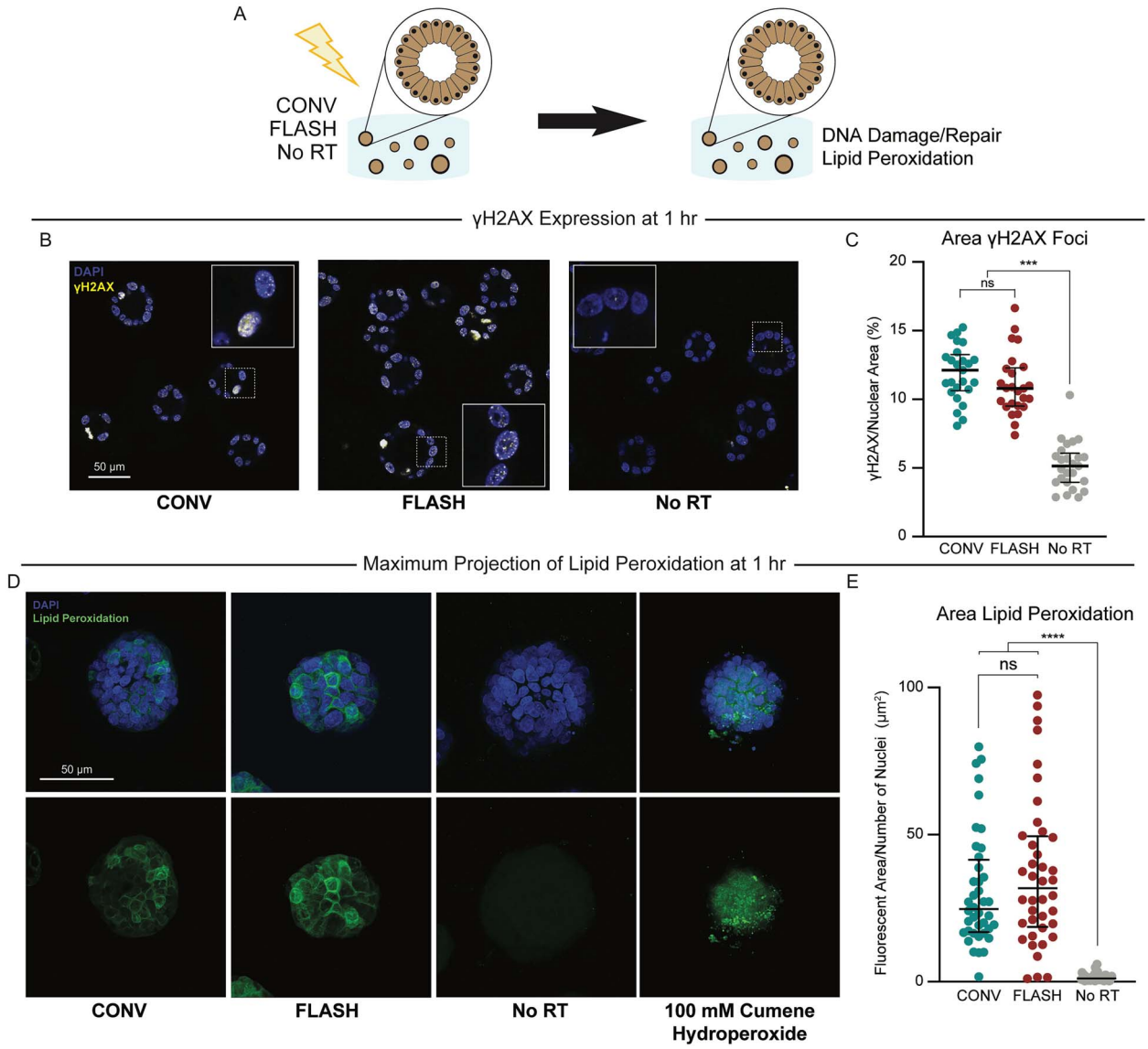

Figure 3. Human enteroid damage and repair response to radiation. (A) Schematic illustrating the radiation of human enteroids that were assayed for DNA damage/repair and lipid peroxidation 1 h after 5 Gy irradiation. (B) Immunocytochemistry of human enteroids stained for the DNA damage response marker γH2AX. Dashed-lines indicate areas of enlargement. (C) Quantification of γH2AX area at 1 h after radiation normalized to nuclear area, n = 25 confocal image stacks across N = 5 independent hydrogel replicates, where each point is a stack of 10 confocal images. (D) Maximum intensity projection images of lipid peroxidation in human enteroids 1 h after radiation. (E) Quantification of lipid peroxidation area normalized to number of nuclei, n = 40 confocal images across N = 4 independent hydrogel replicates, where each point is a single maximum intensity projection. Median with interquartile range, two-tailed unpaired t-tests, **** = $P < 0.0001$, *** = $P < 0.001$, ns = not significant. CONV and FLASH induced statistically similar levels of DNA double-strand breaks and lipid peroxidation compared to the unirradiated control.

Three of the several pathways that had significantly higher expression in the FLASH-irradiated enteroids compared to CONV were genes from the *WNT*-family, cell junction proteins, and genes downstream of hypoxia (Fig. 4G, Fig. S9, Table S3). While we observed minimal differences at 1 h in the expression of several common intestinal stem cell markers (*LGR5, BMI1,* and *OLFM4*), we did see a significant upregulation of the canonical stem cell marker *LGR5* in the CONV enteroids at 96 h. In addition, we observed an upregulation of key intestinal proliferation makers (*SOX9* and *KLF5*) at 96 h in the FLASH enteroids (Fig. S10, [53, 66]. We also observed higher expression of cell junction proteins, including several claudins and cadherins, in the FLASH-irradiated enteroids at 96 h (Fig. S11). In addition, we saw especially high differential expression of the genes *CA9* and *NDRG1* (Fig. 4E and F). Both *NDRG1* and *CA9* were upregulated in the FLASH-irradiated and no-radiation enteroids at 1 h compared to CONV-irradiated, and both genes had continued high expression of both markers at 96 h. *NDRG1* transcription is known to occur in response to hypoxia [67, 68] and has been reported to be involved in a number of cell functions, including DNA repair and restoring epithelial cell-cell adhesion [69]. Like *NDRG1*, *CA9* is also known to be transcribed following hypoxia [70, 71]. CA9 plays a key role in glycolysis, allowing for sustained energy production in a hypoxic state [72]. Similarly, we also saw increased expression of GLUT1 and LDHA, which are both glycolytic genes downstream of hypoxia (Fig. S12).

We also performed gene set (GSEA) and gene ontology (GO-term) enrichment analyses. The GSEA resulted in the significant enrichment of 7 gene sets at 96 h (nominal *P*-value < 1%) (Table S4), including genes associated with hypoxia and apical

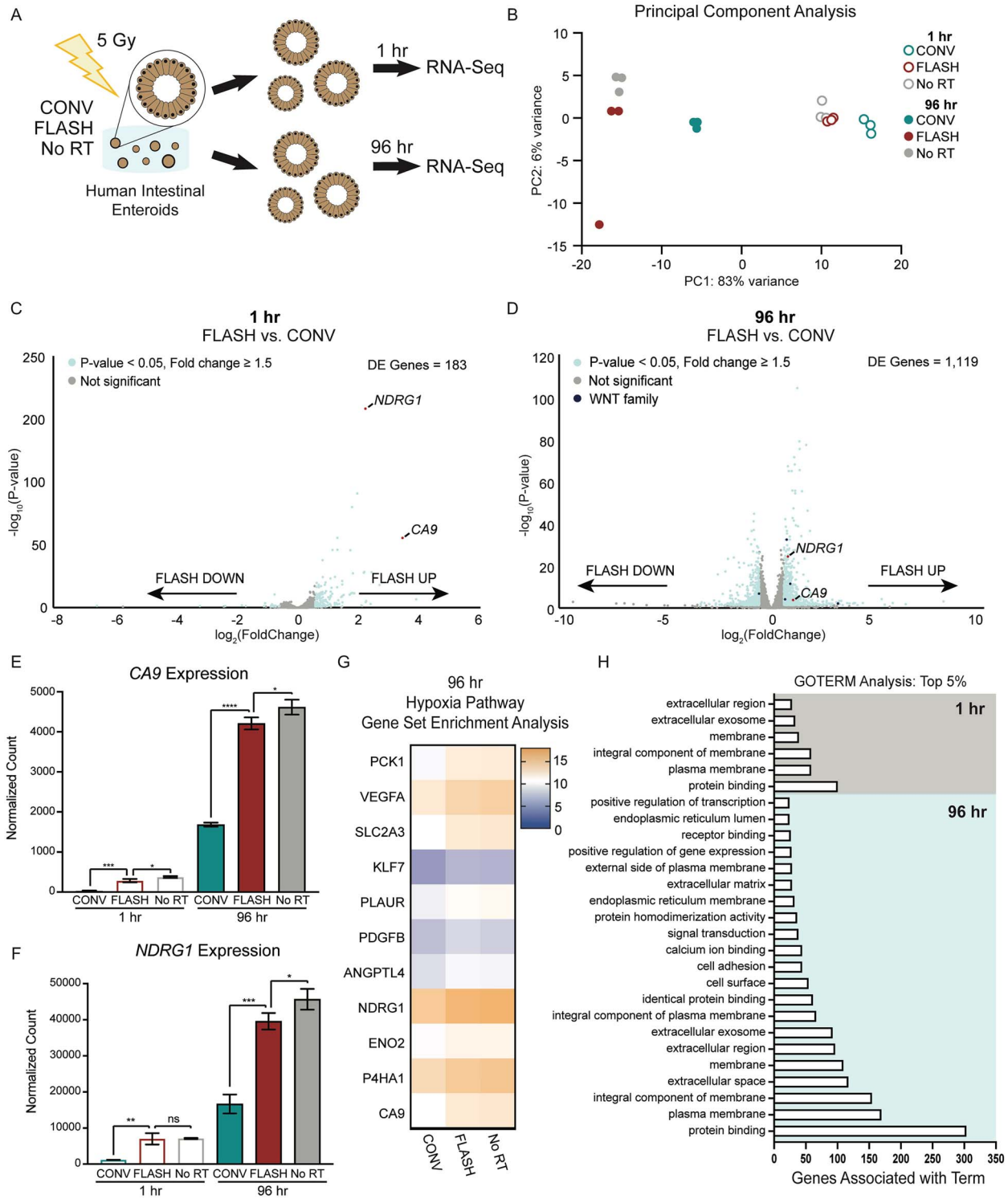

Figure 4. Gene expression of irradiated enteroids. (A) Schematic demonstrating the irradiation of enteroids that were subsequently extracted as whole enteroids and processed for RNA-sequencing. (B) Principal component analysis (PCA) summarizing gene expression across all groups. (C) Volcano plot comparing FLASH enteroids to CONV at 1 h. (D) Volcano plot comparing FLASH enteroids to CONV at 96 h. For C and D, genes in gray are not significantly differentially expressed (DE), while genes in blue are significantly differentially expressed (fold change ≥1.5, $P < 0.05$). Genes of interest that are significantly differentially expressed are marked in red (*NDRG1* and *CA9*) and navy (*WNT*-family genes, panel D only). (E) Expression of the gene *CA9* 1 h and 96 h following radiation. (F) Expression of the gene *NDRG1* 1 h and 96 h after radiation. Two-tailed unpaired t-tests were performed for E and F, n = 3 independent hydrogel replicates, **** = $P < 0.0001$, *** = $P < 0.001$, ** = $P < 0.01$, * = $P < 0.05$, ns = not significant. (G) Heatmap of hypoxia pathway enrichment at 96 h, where expression is displayed as y = $\log_2$(normalized count) for each gene. (H) Top 5% of GOTerms associated with genes significantly upregulated in the FLASH enteroids compared to the CONV group at 1 h (gray) and 96 h (blue). FLASH- and CONV-irradiated enteroids revealed distinct transcriptomic profiles both 1 h and 96 h after irradiation.

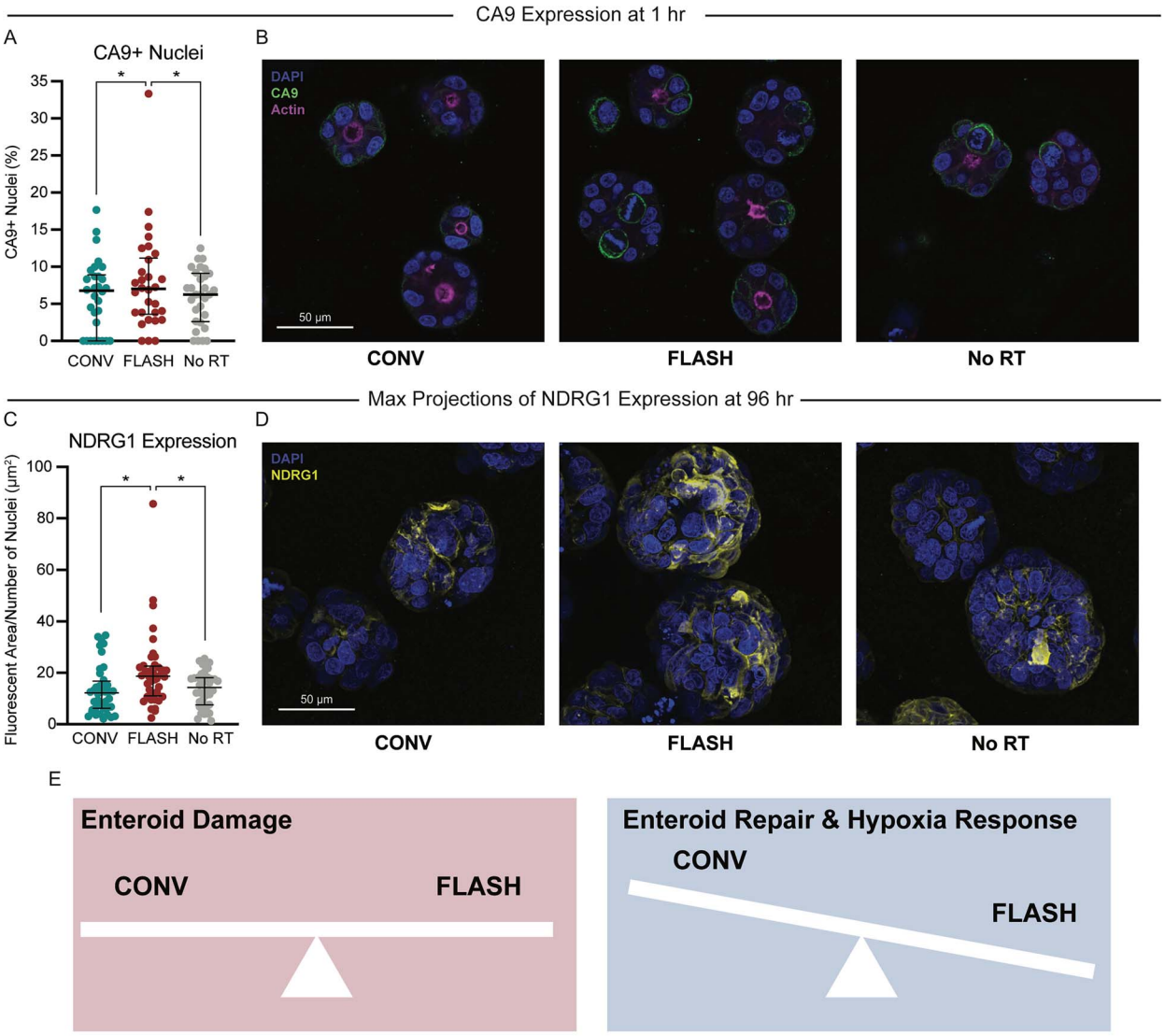

Figure 5. Protein expression of CA9 and NDRG1 hypoxic markers following radiation. (A) Quantification of CA9-positive nuclei, n = 30 confocal images across N = 3 independent hydrogel replicates, where each point is a single confocal image. (B) Immunocytochemistry of enteroids after radiation for the marker CA9 with actin (phalloidin) and nuclei (DAPI) counterstains. (C) Quantification of NDRG1-positive area normalized to number of nuclei, n = 40 confocal images across N = 4 independent hydrogel replicates, where each point is a single maximum intensity projection. Median with interquartile range, two-tailed unpaired t-tests, * = $P < 0.05$. (D) Immunocytochemistry of enteroids stained for the marker NDRG1 with nuclei (DAPI) counterstains. (E) Illustration summarizing the results observed in the human enteroid model. FLASH-irradiated enteroids resulted in increased expression of CA9 and NDRG1, two hypoxia-response proteins.

surface markers (Fig. 4E). The GO-term analysis demonstrated an enrichment of terms across hierarchies (Biological Process, Cellular Component, and Molecular Function) (Fig. 4H). The top 5% of enriched terms included many genes associated with cell membrane and cell adhesion.

FLASH-irradiated enteroids express markers of hypoxia at higher levels than CONV-irradiated enteroids

We next wanted to determine whether the gene expression of *CA9* and *NDRG1* observed through RNA-sequencing resulted in differential protein-level expression of these markers. We again irradiated the enteroids using CONV or FLASH and immunostained for both proteins. We saw a greater number of CA9-positive nuclei following FLASH compared to CONV and the unirradiated enteroids (Fig. 5A and B). This trend was conserved for the marker NDRG1, where we saw greater expression of NDRG1 in the FLASH-irradiated enteroids than the CONV- and unirradiated groups (Fig. 5C and D). These results confirm the up-regulated protein expression of two hypoxia markers, *CA9* and *NDRG1*, for the FLASH intestinal enteroids. Taken together, these results demonstrate similar levels of DNA and lipid damage across FLASH-irradiated and CONV-irradiated enteroids (as measured by γH2AX and lipid peroxidation in Fig. 3), while FLASH-irradiated enteroids displayed greater potential for repair compared to the CONV-irradiated enteroids (as evidenced by enteroid cross-sectional area and morphology in Fig. 2 and *SOX9* expression in Fig. S10) and increased expression of hypoxia markers (as quantified at the mRNA level in Fig. 4 and the protein level in Fig. 5).

DISCUSSION

Previous work has demonstrated the preservation of healthy tissue regeneration after FLASH relative to CONV [21–25, 27], which

may be due to better maintained repair mechanisms. However, understanding the effects of FLASH on human-specific tissue is imperative to fully realizing the therapeutic potential of this alternative approach to radiation delivery. In this study, we intentionally used undifferentiated, early-stage enteroids to capture the response of the most radio-sensitive portion of the intestines: the highly proliferative small intestinal crypt [65]. Previous murine studies demonstrated an increase in intestinal crypt regeneration following FLASH compared to CONV [21–25, 73]. Our irradiated murine enteroids demonstrated a similar result, where we saw an improvement with FLASH in enteroid recovery following radiation, as measured by enteroid size and morphology in a colony formation assay. Similar to our murine enteroid observations, the FLASH-irradiated human cells were more likely to form enteroids with a larger cross-sectional area and polarized morphology in the colony formation assay compared to the CONV-irradiated group. To the best of our knowledge, this study is the first of its kind to irradiate healthy, human intestinal enteroids with FLASH. Taken together, our data validate this *in vitro* model system as a tractable platform to explore the mechanisms underlying the FLASH effect within human cultures.

We leveraged the accessibility of the enteroid model to explore the gene- and protein-level responses of the human tissue to CONV and FLASH. Our observations of enteroid damage (through the quantification of γH2AX localization and lipid peroxidation) suggested that damage between the CONV and FLASH was not significantly different. This is in agreement with a study that irradiated human epithelial cells and observed equal expression of the marker 53BP1, a marker for DNA double strand breaks, between CONV and FLASH [26]. However, other studies suggest a difference in damage following CONV compared to FLASH may occur. Specifically, previous *in vivo* murine radiation demonstrated a modest reduction of γH2AX foci per intestinal stem cell at 12 h after FLASH compared to CONV [21]. These differences may be attributed to the temporal dynamics of DNA damage repair; here we evaluated γH2AX localization 1 h following radiation. Further studies at earlier and later time-points along with alternative methods of studying DNA repair [74] will be helpful in the future to quantify the rate of DNA repair across radiation modalities and provide a clearer answer as to whether FLASH results in less DNA damage and/or promotes a more efficient DNA repair response. Similarly, our studies did not observe differences in lipid damage, as quantified by a lipid peroxidation assay. Thus, in our *in vitro* human enteroid model, we saw that FLASH resulted in similar levels of damage to healthy tissue as CONV.

In contrast to their comparable DNA and lipid damage, our *in vitro* human enteroids displayed significantly increased repair responses after FLASH exposure compared to CONV. Specifically, FLASH-irradiated enteroids demonstrated an increased expression of several stemness genes (including *WNT*-family genes, *SOX9*, and *KLF5*) and more rapid enteroid growth. These data are consistent with previous studies in mouse models, where intestinal crypt regeneration was more frequently observed following FLASH [21, 22]. Interestingly, at the 5 Gy dose used throughout most of this study, gene expression of several intestinal stem cell markers (*LGR5* and *BMI1*) was unaltered at 1 h by either CONV or FLASH, suggesting that this dose is not high enough to ablate intestinal stem cells. These data suggest that the overall number of stem/progenitor cells may be similar in FLASH and CONV; however, FLASH may stimulate stem/progenitor cells to more actively divide and induce new tissue regeneration. This would explain the significant increase in *SOX9* and *KLF5* expression that we observed following FLASH. An emerging hypothesis that is supported by our data is that the higher dose rate of FLASH compared to CONV may activate the stem cell niche to induce proliferation and repair mechanisms, which we hypothesize may play a role in the differences in enteroid size that we observed between CONV, FLASH, and the unirradiated control. Other studies have demonstrated that low doses of irradiation can result in increased cell proliferation in healthy murine and human cells [75–77] thus, this is an exciting direction for future mechanistic studies.

In addition to an increase in enteroid repair following FLASH, our data also demonstrated differences in enteroid structure and cell-cell adhesion following CONV and FLASH. First, we observed that while CONV enteroids frequently had an aberrant morphology, FLASH enteroids displayed morphologies that were statistically similar to unirradiated enteroids, as quantified by enteroid roundness for murine cultures and proper polarization for human cultures. Consistent with these morphological observations, we saw statistically higher expression of cell adhesion- and cell membrane-associated genes (including several claudins and cadherins and tight junction protein 3) for FLASH and unirradiated controls compared to CONV human enteroids. These findings are consistent with murine *in vivo* studies that described the maintenance of tight junction protein expression in the brain and improved epithelial barrier integrity of the gut following FLASH [21, 78].

The relationship between FLASH and hypoxia has been extensively studied previously [46–48, 50, 79–81]. This is especially relevant for our three-dimensional enteroid cultures, as embedded tissue culture of intestinal organoids are known to be hypoxic [82]. Compared to the unirradiated control, the FLASH-irradiated enteroids demonstrated maintenance of hypoxia-related gene expression following FLASH, while we saw lower levels of hypoxia-associated gene expression in the CONV group. In addition, we saw decreased expression of genes critical to glycolysis, which are directly downstream of cellular hypoxia [83], in the CONV-irradiated enteroids. This may suggest that CONV disrupts normal cell metabolism, leading to reduced levels of oxygen consumption, which would explain the lower levels of hypoxia-associated gene expression in the CONV-irradiated enteroids. Interestingly, while we observed statistically similar gene expression of *CA9* and *NDRG1* between the FLASH and unirradiated enteroids, we saw an increased expression of these two markers in the FLASH-irradiated group when quantifying protein expression. These differences between mRNA transcription and protein translation may be a result of the highly complex gene expression regulation that occurs during cellular response to stress, when post-transcriptional responses to stress can lead to deviations in gene and protein expression [84, 85]. Additional studies are needed to evaluate the specific role(s) of hypoxia-associated proteins following CONV and FLASH, such as through immunostaining of HIF1 and the use of HIF1 inhibitors; evaluate whether the increase in glycolytic gene expression assists with cell proliferation and repair; and quantify DNA damage over time. These types of mechanistic studies would be enabled by the experimental tunability available in this *in vitro* human tissue culture model.

This work focused primarily on a single dose-rate (FLASH: 113.1 Gy/s and CONV: <0.2 Gy/s) at a total dose of 5 Gy. Future work can explore if the differences between FLASH and CONV are maintained across dose rates to identify the optimal protocols for human therapy. While enteroids are powerful tools to elucidate many of the human-specific cellular and molecular-level differences between CONV and FLASH, these structures are inherently simplified. In particular, this enteroid system contains only the intestinal epithelium, making it well suited to answer

mechanistic questions about stem and progenitor cell responses to FLASH. However, this current enteroid system is not able to test hypotheses related to immune or vascular system interactions, which are also hypothesized to play a role in FLASH responses [78, 86, 87]. More complex engineered *in vitro* models (such as microphysiological systems) are currently being developed to incorporate advances in microfluidics, bioprinting, and biomaterials [88–92]. In addition, while our *in vitro* enteroid model contained only healthy human epithelium, future models could incorporate primary cancer enteroids (or tumoroids), including human cancer cell lines that have already been validated for FLASH experimentation [47, 93–100]. In fact, our previous work demonstrated the utility of human lung tumor spheroids for CONV and FLASH radiation experiments [100]. In the future, we envision that the integrated knowledge gained from complementary use of a multitude of model systems (including *in vitro* healthy and cancer human organoid models, engineered microphysiological systems, and preclinical animal models) will be critical to understanding the mechanisms driving the FLASH-effect and the potential translation of this therapeutic modality to improve patient quality of life.

EXPERIMENTAL PROCEDURES

Resource availability

Further information and requests for resources and reagents should be directed to and will be fulfilled by the corresponding author, Sarah Heilshorn (heilshorn@stanford.edu).

Software and data availability

All coding was completed using R-studio. The R-script used to analyze the RNA-sequencing data followed the open-source Bioconductor DESeq2 workflow: Love *et al*. [101].

The RNA-sequencing files will be uploaded through the NCBI Gene Expression Omnibus database and will be available open-access. Additional data incorporated into this article will be shared on reasonable request to the corresponding author.

Murine and human enteroid passaging and maintenance culture

Human primary intestinal enteroids were maintained for ≤25 passages across all experiments. Cells were encapsulated in 40 μl domes of basement membrane extract matrix, specifically Cultrex Basement Membrane Extract-Reduced Growth Factor (BME-RGF) Type 2 (Bio-Techne, Minneapolis, MN) within 24-well plates. Enteroids were passaged once confluent (∼every 1–2 weeks). To remove the enteroids from the matrix, Cultrex domes were flushed with pre-chilled, 5 mM ethylenediamine tetraacetic acid (EDTA) in phosphate buffered saline (PBS) and centrifuged for 5 min at 500 × *g*. Following aspiration of the supernatant, the enteroid pellet was resuspended in Tryp-LE (Thermo Fisher Scientific, Waltham, MA) and incubated at 37°C for 10 min, with pipette-mixing every 5 min to dissociate the enteroids into single cells. The Tryp-LE was then quenched with enteroid maintenance media (described below), and centrifuged for 5 min at 500 × *g*. The quenched solution was then aspirated and the cell pellet was resuspended in fresh media for counting. The pellet was centrifuged one final time at 5 min at 500 × *g* at the desired cell concentration (750 000 cells/ml for maintenance cultures) and resuspended in pre-chilled Cultrex. After a 10 min incubation at 37°C, 750 ul of enteroid maintenance media was added to each well. Small molecule inhibitors, 10 μM Y-27632 and 2.5 μM CHIR-99021 (Cayman Chemical, Ann Arbor, MI), were added to the first media change of each maintenance culture. Media was refreshed every 2–4 days, depending on confluence.

Enteroid growth medium generation

Enteroid growth media was prepared using a 1:1 mixture of ADMEM/F-12 (Thermo Fisher Scientific, Waltham, MA) with L-WRN cell (ATCC CRL3276) conditioned media. Conditioned media was prepared by plating L-WRN cells on T150 flasks in L-WRN growth media (Dulbecco's Modified Essential Medium (DMEM) supplemented with 10% FBS and 1% penicillin-streptomycin-glutamine (PSQ)). Cells were passaged 2 days after seeding and split at 1:4 ratio. Growth media was replaced with selection media (L-WRN growth medium supplemented with G418 and hygromycin (500 μg/ml)) 1 day after seeding to select for cells expressing Wnt-3A, R-spondin 3, and Noggin. Cells were expanded for 2 additional passages and then cultured with L-WRN collection media (ADMEM/F12 with 10% FBS and 1% PSQ) for 3 days, with media being collected and refreshed every 24 h. Collection media was then mixed in a 1:1 ratio with ADMEM/F-12 and supplemented with the following: 1 mM HEPES (Thermo Fisher Scientific, Waltham, MA), 1× Glutamax (Thermo Fisher Scientific, Waltham, MA), 10 mM nicotinamide (Sigma-Aldrich, St. Louis, MO), 1 mM N-acetylcysteine (Sigma-Aldrich, St. Louis, MO), 1× B-27 supplement (Thermo Fisher Scientific, Waltham, MA), 0.5 μM A83-01 (Sigma-Aldrich, St. Louis, MO), 1× PSQ (Thermo Fisher Scientific, Waltham, MA), 10 nM Gastrin-I (Sigma-Aldrich, St. Louis, MO), 10 μM SB-202190 (Thermo Fisher Scientific, Waltham, MA), 50 ng/ml recombinant EGF (Thermo Fisher Scientific, Waltham, MA), and 1× Normocin (InvivoGen, San Diego, CA).

Enteroid differentiation

Human primary intestinal cells were encapsulated in 10 μl domes of Cultrex Basement Membrane Extract-Reduced Growth Factor (BME-RGF) Type 2 (Bio-Techne, Minneapolis, MN) on glass 96-well plates (Cellvis, Mountain View, CA) for differentiation. For a period of 10 days, 200 μl of L-WRN collection media was added to each well for initial enteroid formation. Media was refreshed every third day. Following the growth period, each well was treated with 200 μl of IntestiCult™ Human Organoid Growth Medium (STEMCELL Technologies, Vancouver, BC) and 5 μM DAPT (STEMCELL Technologies, Vancouver, BC) every 2 days for an additional 10 days (20 days total).

Immunocytochemistry

Enteroids cultured for immunostaining were either seeded within silicone molds adhered to glass coverslips or using dome culture on glass 96-well plates (Cellvis, Mountain View, CA). Cells were fixed with pre-warmed 4% paraformaldehyde (PFA) in PBS and incubated at room temperature for 30–45 min depending on the volume of the gels. The PFA was removed and three 5-min PBS washes were completed. Enteroids were permeabilized for 1 h at room temperature with 0.25% v/v Triton X-100 in PBS (PBST). Enteroids were subsequently blocked with 5 wt% bovine serum albumin (BSA), 5% v/v goat or donkey serum, and 0.5% v/v Triton X-100 in PBS for 3 h on a rocker. Primary antibodies were prepared using the dilutions listed in Table 1 and were diluted with 2.5 wt% BSA, 2.5% v/v goat serum, and 0.5% v/v Triton X-100 in PBS (Antibody Dilution Solution). Enteroids were incubated with primary antibodies overnight at 4°C. Enteroids were then washed with PBST three times, 60 min each. Secondary solutions were diluted at 1:500 in Antibody Dilution Solution and incubated overnight at 4°C in the dark. Enteroids were again washed with

Table 1. Antibody information.

Target	Species	Vendor	Product #	Dilution
ZO-1	Mouse	Invitrogen	33-9100	1:150
β-catenin	Rabbit	Cell Signal. Tech	8480	1:150
LYZ	Rabbit	Invitrogen	PA5-16668	1:100
CHGA	Rabbit	Invitrogen	PA5-85952	1:200
Actin/Phalloidin	N/A—preconjug.	Invitrogen	A22284	1:100–200
Ki67	Rabbit	Cell Signal. Tech	12202	1:200
SOX9	Mouse	Human Prot. Atlas	AMAb90795	10 μg/ml
FABP1	Mouse	BioTechne	MAB29641	1:200
γH2AX	Mouse	Abcam	ab26350	1:200
CA9	Mouse	Abcam	ab107257	1:300
NDRG1	Rabbit	VWR	76044-940	1:50

PBST three times, 30 min each. A 1:2000 dilution of DAPI and 1:100-200 dilution of phalloidin was then prepared and applied to the cells for 1.5 h. The enteroids were washed three additional times, 10 min each, with PBST. Samples prepared on coverslips were then dried and a drop of ProLong Gold Antifade (Thermo Fisher Scientific, Waltham, MA) mounting media was applied to adhere to another coverslip. Mountant was allowed to cure overnight at room temperature. Fresh PBS was applied to enteroids in 96-well plates. Images were taken using a Stellaris confocal microscope (Leica, Wetzlar, Germany).

Enteroid irradiation

Murine and human enteroids were seeded in 6-, 24-, or 96-well plates in the dome cultures described above and allowed to grow for 6–7 days. The plates were then placed within a Varian Trilogy (Varian Medical Systems) clinical linear accelerator that has been configured for *in vitro* radiation, as previously described [102]. For the CONV irradiations, the plates were positioned at a distance of 82.2 cm from the scattering foil and irradiated with a 15.7 MeV open field electron beam. For FLASH irradiations, the plates were positioned at a distance of 29.2 cm from the scattering foil and irradiated with a 16.6 MeV open field electron beam. The radiation field for FLASH at this distance has 5% flatness at a circular radius of 4 cm from the center of the beam, which uniformly covers the seeded wells of the well-plates (Fig. S1A and B). The absorbed surface doses (entrance doses) were measured by mounting radiochromic film (EBT3, Ashland, USA) beneath each plate (Fig. S1C). The entrance doses confirmed an average of 2.2 and 2.0% deviation from the prescribed dose for CONV and FLASH respectively, and an average of 0.09 Gy difference between CONV and FLASH irradiated groups (Fig. 1B, Fig. S1D). All FLASH radiations were performed using 1 Gy per pulse at dose rates above 100 Gy/s, whereas CONV dose rates were below 0.19 Gy/s. Detailed irradiation parameters are presented at Table S1.

Live/dead assay

Murine enteroids were seeded, cultured, and irradiated as described above. Following irradiation, media from each well was replaced with 300 μl of live/dead staining solution. Live/dead staining solution was prepared using 2 μM calcein-AM and 4 μM ethidium homodimer-1 in PBS (Thermo Fisher Scientific, Waltham, MA). Enteroids were incubated for 15 min at 37°C. One PBS wash was performed and fresh PBS was maintained on the samples for imaging.

Hypoxia probe assay

Enteroids were seeded and cultured as described above. The Invitrogen Image-iT™ Green Hypoxia Reagent Kit (Thermo Fisher Scientific, Waltham, MA) was used to measure levels of hypoxia in the cultures. Briefly, the hypoxia reagent was added to each well at a concentration of 10 μM in WENR media. Enteroids were then incubated at 37°C for 1 h. Following incubation, enteroids were protected from light and fixed with 4% PFA in PBS at room temperature for 30 min. The enteroids were then washed once with PBS and fresh PBS was added for imaging. Images were taken using a Stellaris confocal microscope (Leica, Wetzlar, Germany).

Enteroid growth, roundness, and ZO-1 analysis

Brightfield images were taken at 10× magnification every 2 days to observe enteroid growth over time. Three z-slice images were taken across 3 locations in each well across all time-points. To analyze enteroid growth, enteroids were traced and their corresponding surface area was measured using FIJI (ImageJ, NIH). A threshold of 1000 μm^2 was used to consider an enteroid formed. The FIJI Roundness measurement tool was used to capture the roundness of each enteroid. Roundness measurements were averaged across all enteroids in each well. Enteroids were stained with ZO-1 and imaged, as described above. ZO-1 positivity was quantified as a binary "1" if the enteroid lumen was positive for ZO-1 or "0" if the enteroid did not express ZO-1 in the expected lumen-area. The percentage of enteroids with ZO-1-positive lumens was averaged per well and reported relative to the no-radiation control.

Lipid peroxidation assay

The Click-iT™ Lipid Peroxidation Imaging Kit was used to quantify lipid peroxidation in the enteroids (Thermo Fisher Scientific, Waltham, MA). Briefly, enteroids were treated with the Click-iT LAA stock solution for 1 h prior to radiation and incubated at 37°C. The cells were radiated and subsequently washed 3 times for 5 min each. The positive control was treated with cumene hydroperoxide for 2 h. The enteroids were then fixed with 4% PFA in PBS at room temperature for 30 min and washed with 0.5% Triton X-100. Enteroids were then blocked with 1% BSA in PBS for 30 min at room temperature. The Click-iT reaction cocktail was then added and the enteroids were allowed to incubate for 30 min at room temperature in the dark. Enteroids were then stained with DAPI, as described above, for 10 min. Enteroids were washed with PBS and fresh PBS was replaced for imaging. Images were taken using a Stellaris confocal microscope (Leica, Wetzlar, Germany). Lipid peroxidation area quantification was performed using FIJI. Thresholds were set for each maximum projection to capture the fluorescent area of each enteroid. That area was then normalized to the area of nuclei in each enteroid, allowing the quantification of fluorescent area per nuclei. Nuclei were quantified using CellProfiler (Cambridge, Massachusetts). Briefly,

each z-stack containing 10 slices was loaded into CellProfiler, grouped according to its specific stack, and tracked through the entirety of the enteroid width. This allowed the quantification of nuclei throughout the z-plane of the enteroid.

γH2AX imaging and quantification

Enteroids were radiated, stained, and imaged as described above for both γH2AX and DAPI. Z-stacks containing 10 slices per image were loaded into CellProfiler. Area of foci and nuclear area was quantified for each slice and averaged across each hydrogel, allowing the area of foci to be normalized to the area of nuclei.

RNA-sequencing of Enteroids

Enteroids were cultured and radiated as described above. Following radiation (at either 1 h or 96 h), enteroids were removed from Cultrex matrices by flushing the domes with pre-chilled 5 mM EDTA. Enteroids were then centrifuged at 300 × *g* for 5 min to pellet the enteroids. The Cultrex/EDTA supernatant was aspirated and the enteroids were flash-frozen in liquid nitrogen. The enteroids were then shipped on dry ice for RNA-extraction, quality control checks, library preparation, and sequencing (Illumina, single index, PolyA selection, 20–30 million reads per sample) (Azenta Life Sciences, Burlington, MA). Data analysis was performed using R-studio and followed the Bioconductor DESeq2 workflow.

GOTerm and GSEA analyses

GOTerm and GSEA analyses were performed using the normalized counts obtained from the RNA-sequencing data, described above. DAVID2021 (Laboratory of Human Retrovirology and Immunoinformatics, National Institutes of Health) was used to perform the GOTerm analysis. All genes with a $P < 0.05$ and a fold change ≥1.5 were uploaded to the gene list. The GOTerm analysis included genes across the biological process, cellular component, and molecular function categories. The top 5% of terms were reported. The GSEA analysis was performed using the GSEA software (UC San Diego and Broad Institute) and the MSigDB.v2023.Hs chip platform. 1000 permutations were performed per run.

CA9 and NDRG1 imaging and quantification

Enteroids were radiated, stained, and imaged as described above. The number of CA9-positive nuclei was recorded through the width of each enteroid. This number was then normalized to the number of nuclei present throughout each z-stack. The quantification of NDRG1 area was carried out using FIJI. For each maximum projection, specific thresholds were established to capture the fluorescent area of each enteroid. This area was normalized to the area of nuclei within each enteroid, enabling the measurement of fluorescent area per nuclei. The quantification of nuclei for both the CA9 and NDRG1 analysis was performed using CellProfiler. Each z-stack consisting of 10 slices was imported into CellProfiler. The stacks were grouped according to their respective stack and tracked across the entire width of the enteroid. This approach facilitated the quantification of nuclei throughout the z-plane of the enteroid.

Statistical analysis

The following statistical significance representation is used for all significance testing in this publication: $^{*} = P < 0.05$, $^{**} = P < 0.01$, $^{***} = P < 0.001$, $^{****} = P < 0.0001$. Data was analyzed using a two-tailed Student's t-test. All statistical analysis was performed using GraphPad Prism 9.0 software (GraphPad Software, La Jolla, CA, USA).

Author contributions

K.C.K., B.C.M.V., and V.S.V. designed, executed, and analyzed experiments. S.M., V.V., R.M., M.R.A., and L.S. performed radiations. B.L. and S.D. prepared necessary resources for radiations. K.C.K. and S.C.H. wrote the manuscript, with input from all co-authors. S.C.H., B.W.L., and E.B.R. supervised the study.

Funding

This work was supported by the California Institute for Regenerative Medicine (DISC2-13020 to S.C.H.) and the National Institutes of Health (R01EB027666 to S.C.H. and R01CA233958 to B.W.L.). We also gratefully acknowledge the generous support of philanthropic donors to the Department of Radiation Oncology, Stanford University School of Medicine. The authors would also like to thank the National Science Foundation (NSF) Graduate Research Fellowship Program awarded to K.C.K. and the National Institutes of Health training grant T32GM119995. The authors would also like to acknowledge the Stanford Materials Science and Engineering Research Experience for Undergraduates and the Stanford Bioengineering Research Experience for Undergraduates for their financial support. Part of this work was performed at the Stanford Nano Shared Facilities (SNSF), supported by the National Science Foundation under award ECCS-2026822.

Supplementary data

Supplementary data is available at *INTBIO Journal* online.

Conflict of interest statement. B.W.L. is a co-founder and board member of TibaRay, is a consultant on a clinical trial steering committee for BeiGene, and has received lecture honorarium from Mevion, outside the submitted work.

Data availability

All data included within this article will be shared upon reasonable request to the corresponding author.

References

1. Baskar R, Itahana K. Radiation therapy and cancer control in developing countries: can we save more lives? *Int J Med Sci* 2017;**14**:13–7.
2. Chen G, Han Y, Zhang H et al. Radiotherapy-induced digestive injury: diagnosis, treatment and mechanisms. *Front Oncol* 2021;**11**:757973.
3. Giuranno L, Ient J, De Ruysscher D et al. Radiation-induced lung injury (RILI). *Front Oncol* 2019;**9**:877.
4. Hauer-Jensen M, Denham JW, Andreyev HJ. Radiation enteropathy—pathogenesis, treatment and prevention. *Nat Rev Gastroenterol Hepatol* 2014;**11**:470–9.
5. Phillips GS, Freret ME, Friedman DN et al. Assessment and treatment outcomes of persistent radiation-induced alopecia in patients with cancer. *JAMA Dermatol* 2020;**156**:963–72.
6. Stacey R, Green JT. Radiation-induced small bowel disease: latest developments and clinical guidance. *Ther Adv Chronic Dis* 2014;**5**:15–29.
7. Wang H, Wei J, Zheng Q et al. Radiation-induced heart disease: a review of classification, mechanism and prevention. *Int J Biol Sci* 2019;**15**:2128–38.

8. Shadad AK, Sullivan FJ, Martin JD et al. Gastrointestinal radiation injury: symptoms, risk factors and mechanisms. *World J Gastroenterol* 2013;**19**:185–98.
9. Classen J, Belka C, Paulsen F et al. Radiation-induced gastrointestinal toxicity. Pathophysiology, approaches to treatment and prophylaxis. *Strahlenther Onkol* 1998;**174**:82–4.
10. Spit M, Koo BK, Maurice MM. Tales from the crypt: intestinal niche signals in tissue renewal, plasticity and cancer. *Open Biol* 2018;**8**:180120.
11. Matuszak N, Suchorska WM, Milecki P et al. FLASH radiotherapy: an emerging approach in radiation therapy. *Rep Pract Oncol Radiother* 2022;**27**:343–51.
12. Sakaguchi M, Maebayashi T, Aizawa T et al. Patient outcomes of monotherapy with hypofractionated three-dimensional conformal radiation therapy for stage T2 or T3 non-small cell lung cancer: a retrospective study. *Radiat Oncol* 2016;**11**:3.
13. Hong TS, Ritter MA, Tome WA et al. Intensity-modulated radiation therapy: emerging cancer treatment technology. *Br J Cancer* 2005;**92**:1819–24.
14. Sterzing F, Engenhart-Cabillic R, Flentje M et al. Image-guided radiotherapy: a new dimension in radiation oncology. *Dtsch Arztebl Int* 2011;**108**:274–80.
15. Chmura S, Winter KA, Robinson C et al. Evaluation of safety of stereotactic body radiotherapy for the treatment of patients with multiple metastases: findings from the NRG-BR001 phase 1 trial. *JAMA Oncol* 2021;**7**:845–52.
16. Feng FY, Kim HM, Lyden TH et al. Intensity-modulated radiotherapy of head and neck cancer aiming to reduce dysphagia: early dose-effect relationships for the swallowing structures. *Int J Radiat Oncol Biol Phys* 2007;**68**:1289–98.
17. Wang-Chesebro A, Xia P, Coleman J et al. Intensity-modulated radiotherapy improves lymph node coverage and dose to critical structures compared with three-dimensional conformal radiation therapy in clinically localized prostate cancer. *Int J Radiat Oncol Biol Phys* 2006;**66**:654–62.
18. Lo SS, Fakiris AJ, Chang EL et al. Stereotactic body radiation therapy: a novel treatment modality. *Nat Rev Clin Oncol* 2010;**7**:44–54.
19. Tipton K, Launders JH, Inamdar R et al. Stereotactic body radiation therapy: scope of the literature. *Ann Intern Med* 2011;**154**:737–45.
20. Favaudon V, Caplier L, Monceau V et al. Ultrahigh dose-rate FLASH irradiation increases the differential response between normal and tumor tissue in mice. *Sci Transl Med* 2014;**6**:245ra93, 1–9.
21. Levy K, Natarajan S, Wang J et al. Abdominal FLASH irradiation reduces radiation-induced gastrointestinal toxicity for the treatment of ovarian cancer in mice. *Sci Rep* 2020;**10**:21600.
22. Valdes Zayas A, Kumari N, Liu K et al. Independent reproduction of the FLASH effect on the gastrointestinal tract: a multi-institutional comparative study. *Cancers (Basel)* 2023;**15**:2121.
23. Eggold JT, Chow S, Melemenidis S et al. Abdominopelvic FLASH irradiation improves PD-1 immune checkpoint inhibition in preclinical models of ovarian cancer. *Mol Cancer Ther* 2022;**21**:371–81.
24. Kim MM, Verginadis II, Goia D et al. Comparison of FLASH proton entrance and the spread-out Bragg peak dose regions in the sparing of mouse intestinal crypts and in a pancreatic tumor model. *Cancers (Basel)* 2021;**13**:4244.
25. Diffenderfer ES, Verginadis II, Kim MM et al. Design, implementation, and in vivo validation of a novel proton FLASH radiation therapy system. *Int J Radiat Oncol Biol Phys* 2020;**106**:440–8.
26. Shi X, Yang Y, Zhang W et al. FLASH X-ray spares intestinal crypts from pyroptosis initiated by cGAS-STING activation upon radioimmunotherapy. *Proc Natl Acad Sci U S A* 2022;**119**:e2208506119.
27. Zhu H, Xie D, Yang Y et al. Radioprotective effect of X-ray abdominal FLASH irradiation: adaptation to oxidative damage and inflammatory response may be benefiting factors. *Med Phys* 2022;**49**:4812–22.
28. Bourhis J, Sozzi WJ, Jorge PG et al. Treatment of a first patient with FLASH-radiotherapy. *Radiother Oncol* 2019;**139**:18–22.
29. Mascia AE, Daugherty EC, Zhang Y et al. Proton FLASH radiotherapy for the treatment of symptomatic bone metastases: the FAST-01 nonrandomized trial. *JAMA Oncol* 2023;**9**:62–9.
30. Hartung T. Thoughts on limitations of animal models. *Parkinsonism Relat Disord* 2008;**14**:S81–3.
31. Fujii M, Matano M, Toshimitsu K et al. Human intestinal organoids maintain self-renewal capacity and cellular diversity in niche-inspired culture condition. *Cell Stem Cell* 2018;**23**:787–793.e6.
32. Parikh K, Antanaviciute A, Fawkner-Corbett D et al. Colonic epithelial cell diversity in health and inflammatory bowel disease. *Nature* 2019;**567**:49–55.
33. Sugimoto S, Sato T. Organoid vs in vivo mouse model: which is better research tool to understand the biologic mechanisms of intestinal epithelium? *Cell Mol Gastroenterol Hepatol* 2022;**13**:195–7.
34. Nicholson AM, Olpe C, Hoyle A et al. Fixation and spread of somatic mutations in adult human colonic epithelium. *Cell Stem Cell* 2018;**22**:909–918.e8.
35. Sato T, Stange DE, Ferrante M et al. Long-term expansion of epithelial organoids from human colon, adenoma, adenocarcinoma, and Barrett's epithelium. *Gastroenterology* 2011;**141**:1762–72.
36. Nuwer R. US agency seeks to phase out animal testing. *Nature* 2022. https://doi.org/10.1038/d41586-022-03569-9.
37. Lancaster MA, Knoblich JA. Organogenesis in a dish: modeling development and disease using organoid technologies. *Science* 2014;**345**:1247125.
38. Tang XY, Wu S, Wang D et al. Human organoids in basic research and clinical applications. *Signal Transduct Target Ther* 2022;**7**:168.
39. McBride WH, Schaue D. Radiation-induced tissue damage and response. *J Pathol* 2020;**250**:647–55.
40. Azzam EI, Jay-Gerin JP, Pain D. Ionizing radiation-induced metabolic oxidative stress and prolonged cell injury. *Cancer Lett* 2012;**327**:48–60.
41. Su LJ, Zhang JH, Gomez H et al. Reactive oxygen species-induced lipid peroxidation in apoptosis, autophagy, and ferroptosis. *Oxid Med Cell Longev* 2019;**2019**:5080843.
42. Spitz DR, Buettner GR, Petronek MS et al. An integrated physicochemical approach for explaining the differential impact of FLASH versus conventional dose rate irradiation on cancer and normal tissue responses. *Radiother Oncol* 2019;**139**:23–7.
43. Labarbe R, Hotoiu L, Barbier J et al. A physicochemical model of reaction kinetics supports peroxyl radical recombination as the main determinant of the FLASH effect. *Radiother Oncol* 2020;**153**:303–10.
44. Pratx G, Kapp DS. A computational model of radiolytic oxygen depletion during FLASH irradiation and its effect on the oxygen enhancement ratio. *Phys Med Biol* 2019;**64**:185005.
45. Velalopoulou A, Karagounis IV, Cramer GM et al. FLASH proton radiotherapy spares normal epithelial and mesenchymal

tissues while preserving sarcoma response. *Cancer Res* 2021;**81**:4808–21.
46. Montay-Gruel P, Acharya MM, Petersson K et al. Long-term neurocognitive benefits of FLASH radiotherapy driven by reduced reactive oxygen species. *Proc Natl Acad Sci U S A* 2019;**116**:10943–51.
47. Adrian G, Konradsson E, Lempart M et al. The FLASH effect depends on oxygen concentration. *Br J Radiol* 2020;**93**:20190702.
48. Hendry JH, Moore JV, Hodgson BW et al. The constant low oxygen concentration in all the target cells for mouse tail radionecrosis. *Radiat Res* 1982;**92**:172–81.
49. Ling CC, Michaels HB, Epp ER et al. Oxygen diffusion into mammalian cells following ultrahigh dose rate irradiation and lifetime estimates of oxygen-sensitive species. *Radiat Res* 1978;**76**:522–32.
50. Pawelke J, Brand M, Hans S et al. Electron dose rate and oxygen depletion protect zebrafish embryos from radiation damage. *Radiother Oncol* 2021;**158**:7–12.
51. Hauer-Jensen M, Wang J, Boerma M et al. Radiation damage to the gastrointestinal tract: mechanisms, diagnosis, and management. *Curr Opin Support Palliat Care* 2007;**1**:23–9.
52. Co JY, Margalef-Catala M, Monack DM et al. Controlling the polarity of human gastrointestinal organoids to investigate epithelial biology and infectious diseases. *Nat Protoc* 2021;**16**:5171–92.
53. Bastide P, Darido C, Pannequin J et al. Sox9 regulates cell proliferation and is required for Paneth cell differentiation in the intestinal epithelium. *J Cell Biol* 2007;**178**:635–48.
54. Formeister EJ, Sionas AL, Lorance DK et al. Distinct SOX9 levels differentially mark stem/progenitor populations and enteroendocrine cells of the small intestine epithelium. *Am J Physiol Gastrointest Liver Physiol* 2009;**296**:G1108–18.
55. de la Cruz Bonilla M, Stemler KM, Taniguchi CM et al. Stem cell enriched-epithelial spheroid cultures for rapidly assaying small intestinal radioprotectors and radiosensitizers in vitro. *Sci Rep* 2018;**8**:15410.
56. Fujimichi Y, Otsuka K, Tomita M et al. Ionizing radiation alters organoid forming potential and replenishment rate in a dose/dose-rate dependent manner. *J Radiat Res* 2022;**63**:166–73.
57. Montenegro-Miranda PS, van der Meer JHM, Jones C et al. A novel organoid model of damage and repair identifies HNF4α as a critical regulator of intestinal epithelial regeneration. *Cell Mol Gastroenterol Hepatol* 2020;**10**:209–23.
58. Jeon W, Jung SY, Lee CY et al. Evaluation of radiation sensitivity differences in mouse liver tumor organoids using CRISPR/Cas9-mediated gene mutation. *Technol Cancer Res Treat* 2023;**22**:15330338231165125.
59. Cheaito K, Bahmad HF, Hadadeh O et al. Establishment and characterization of prostate organoids from treatment-naive patients with prostate cancer. *Oncol Lett* 2022;**23**:6.
60. Sato T, Vries RG, Snippert HJ et al. Single Lgr5 stem cells build crypt-villus structures in vitro without a mesenchymal niche. *Nature* 2009;**459**:262–5.
61. Petersen N, Reimann F, Bartfeld S et al. Generation of L cells in mouse and human small intestine organoids. *Diabetes* 2014;**63**:410–20.
62. Georgakopoulos N, Prior N, Angres B et al. Long-term expansion, genomic stability and in vivo safety of adult human pancreas organoids. *BMC Dev Biol* 2020;**20**:4.
63. Drost J, Karthaus WR, Gao D et al. Organoid culture systems for prostate epithelial and cancer tissue. *Nat Protoc* 2016;**11**:347–58.
64. Kuo LJ, Yang LX. Gamma-H2AX - a novel biomarker for DNA double-strand breaks. *In Vivo* 2008;**22**:305–9.
65. Kim CK, Yang VW, Bialkowska AB. The role of intestinal stem cells in epithelial regeneration following radiation-induced gut injury. *Curr Stem Cell Rep* 2017;**3**:320–32.
66. McConnell BB, Kim SS, Yu K et al. Krüppel-like factor 5 is important for maintenance of crypt architecture and barrier function in mouse intestine. *Gastroenterology* 2011;**141**:1302–1313.e6.
67. Cangul H. Hypoxia upregulates the expression of the NDRG1 gene leading to its overexpression in various human cancers. *BMC Genet* 2004;**5**:27.
68. Kachhap SK, Faith D, Qian DZ et al. The N-Myc down regulated Gene1 (NDRG1) is a Rab4a effector involved in vesicular recycling of E-cadherin. *PloS One* 2007;**2**:e844.
69. Dominick G, Bowman J, Li X et al. mTOR regulates the expression of DNA damage response enzymes in long-lived Snell dwarf, GHRKO, and PAPPA-KO mice. *Aging Cell* 2017;**16**:52–60.
70. van den Beucken T, Koritzinsky M, Niessen H et al. Hypoxia-induced expression of carbonic anhydrase 9 is dependent on the unfolded protein response. *J Biol Chem* 2009;**284**:24204–12.
71. Sedlakova O, Svastova E, Takacova M et al. Carbonic anhydrase IX, a hypoxia-induced catalytic component of the pH regulating machinery in tumors. *Front Physiol* 2014;**4**:400.
72. Pastorekova S, Gillies RJ. The role of carbonic anhydrase IX in cancer development: links to hypoxia, acidosis, and beyond. *Cancer Metastasis Rev* 2019;**38**:65–77.
73. Ruan JL, Lee C, Wouters S et al. Irradiation at ultra-high (FLASH) dose rates reduces acute normal tissue toxicity in the mouse gastrointestinal system. *Int J Radiat Oncol Biol Phys* 2021;**111**:1250–61.
74. Kordon MM, Zarebski M, Solarczyk K et al. STRIDE-a fluorescence method for direct, specific in situ detection of individual single- or double-strand DNA breaks in fixed cells. *Nucleic Acids Res* 2020;**48**:e14.
75. Li W, Wang G, Cui J et al. Low-dose radiation (LDR) induces hematopoietic hormesis: LDR-induced mobilization of hematopoietic progenitor cells into peripheral blood circulation. *Exp Hematol* 2004;**32**:1088–96.
76. Suzuki K, Kodama S, Watanabe M. Extremely low-dose ionizing radiation causes activation of mitogen-activated protein kinase pathway and enhances proliferation of normal human diploid cells. *Cancer Res* 2001;**61**:5396–401.
77. Liang X, Gu J, Yu D et al. Low-dose radiation induces cell proliferation in human embryonic lung fibroblasts but not in lung cancer cells: importance of ERK1/2 and AKT Signaling pathways. *Dose Response* 2016;**14**:1559325815622174.
78. Allen BD, Acharya MM, Montay-Gruel P et al. Maintenance of tight junction integrity in the absence of vascular dilation in the brain of mice exposed to ultra-high-dose-rate FLASH irradiation. *Radiat Res* 2020;**194**:625–35.
79. Weiss H, Epp ER, Heslin JM et al. Oxygen depletion in cells irradiated at ultra-high dose-rates and at conventional dose-rates. *Int J Radiat Biol Relat Stud Phys Chem Med* 1974;**26**:17–29.
80. Michaels HB, Epp ER, Ling CC et al. Oxygen sensitization of CHO cells at ultrahigh dose rates: prelude to oxygen diffusion studies. *Radiat Res* 1978;**76**:510–21.
81. Koch CJ, Kim MM, Wiersma RD. Radiation-chemical oxygen depletion depends on chemical environment and dose rate: implications for the FLASH effect. *Int J Radiat Oncol Biol Phys* 2023;**117**:214–22.
82. DiMarco RL, Su J, Yan KS et al. Engineering of three-dimensional microenvironments to promote contractile behavior in primary intestinal organoids. *Integr Biol (Camb)* 2014;**6**:127–42.

83. Kierans SJ, Taylor CT. Regulation of glycolysis by the hypoxia-inducible factor (HIF): implications for cellular physiology. *J Physiol* 2021;**599**:23–37.
84. Liu Y, Beyer A, Aebersold R. On the dependency of cellular protein levels on mRNA abundance. *Cell* 2016;**165**:535–50.
85. Cheng Z, Teo G, Krueger S et al. Differential dynamics of the mammalian mRNA and protein expression response to misfolding stress. *Mol Syst Biol* 2016;**12**:855.
86. Zhang Y, Ding Z, Perentesis JP et al. Can rational combination of ultra-high dose rate FLASH radiotherapy with immunotherapy provide a novel approach to cancer treatment? *Clin Oncol (R Coll Radiol)* 2021;**33**:713–22.
87. Jin JY, Gu A, Wang W et al. Ultra-high dose rate effect on circulating immune cells: a potential mechanism for FLASH effect? *Radiother Oncol* 2020;**149**:55–62.
88. Nikolaev M, Mitrofanova O, Broguiere N et al. Homeostatic mini-intestines through scaffold-guided organoid morphogenesis. *Nature* 2020;**585**:574–8.
89. Kasendra M, Tovaglieri A, Sontheimer-Phelps A et al. Development of a primary human small intestine-on-a-Chip using biopsy-derived organoids. *Sci Rep* 2018;**8**:2871.
90. Kim HJ, Ingber DE. Gut-on-a-Chip microenvironment induces human intestinal cells to undergo villus differentiation. *Integr Biol (Camb)* 2013;**5**:1130–40.
91. Madden LR, Nguyen TV, Garcia-Mojica S et al. Bioprinted 3D primary human intestinal tissues model aspects of native physiology and ADME/Tox functions. i*Science* 2018;**2**:156–67.
92. Schreurs R, Baumdick ME, Drewniak A et al. In vitro co-culture of human intestinal organoids and lamina propria-derived CD4(+) T cells. *STAR Protoc* 2021;**2**:100519.
93. Cygler J, Klassen NV, Ross CK et al. The survival of aerobic and anoxic human glioma and melanoma cells after irradiation at ultrahigh and clinical dose rates. *Radiat Res* 1994;**140**:79–84.
94. Town CD. Radiobiology. Effect of high dose rates on survival of mammalian cells. *Nature* 1967;**215**:847–8.
95. Nias AH, Swallow AJ, Keene JP et al. Effects of pulses of radiation on the survival of mammalian cells. *Br J Radiol* 1969;**42**:553.
96. Nias AH, Swallow AJ, Keene JP et al. Survival of HeLa cells from 10 nanosecond pulses of electrons. *Int J Radiat Biol Relat Stud Phys Chem Med* 1970;**17**:595–8.
97. Epp ER, Weiss H, Djordjevic B et al. The radiosensitivity of cultured mammalian cells exposed to single high intensity pulses of electrons in various concentrations of oxygen. *Radiat Res* 1972;**52**:324–32.
98. Adrian G, Konradsson E, Beyer S et al. Cancer cells can exhibit a sparing FLASH effect at low doses under normoxic in vitro-conditions. *Front Oncol* 2021;**11**:686142.
99. Tessonnier T, Mein S, Walsh DWM et al. FLASH dose rate helium ion beams: first in vitro investigations. *Int J Radiat Oncol Biol Phys* 2021;**111**:1011–22.
100. Khan S, Bassenne M, Wang J et al. Multicellular spheroids as in vitro models of oxygen depletion during FLASH irradiation. *Int J Radiat Oncol Biol Phys* 2021;**110**:833–44.
101. Love MI, Huber W, Anders S. Moderated estimation of fold change and dispersion for RNA-seq data with DESeq2. *Genome Biol* 2014;**15**:550. 10.1186/s13059-014-0550-8.
102. Schuler E, Trovati S, King G, Lartey F, Rafat M, Villegas M et al. Experimental platform for ultra-high dose rate FLASH irradiation of small animals using a clinical linear accelerator. *Int J Radiat Oncol Biol Phys* 2017;**97**:195–203.